Polym. Bull. (2015) 72:2573–2589
DOI 10.1007/s00289-015-1422-4

ORIGINAL PAPER

# Supercapacitor behaviors of polyaniline/CuO, polypyrrole/CuO and PEDOT/CuO nanocomposites

**Murat Ates[1,2] · Mehmet Akif Serin[1] · Ilker Ekmen[1] · Yavuz N. Ertas[3]**

Received: 27 February 2015 / Revised: 2 April 2015 / Accepted: 30 May 2015 /
Published online: 7 June 2015
© Springer-Verlag Berlin Heidelberg 2015

**Abstract** Polyaniline (PANI)/copper oxide (CuO), poly(3,4-ethylenedioxythiophene) (PEDOT)/CuO and polypyrrole (PPy)/CuO have been synthesized electrochemically on glassy carbon electrode in sodium dodecyl sulfate in sulfuric acid solution as an electroactive material. To our best knowledge, the first report on comparison of supercapacitor behaviors of PANI/CuO, PEDOT/CuO and PPy/CuO nanocomposite films was studied by electrochemical impedance spectroscopy, related to the plots of Nyquist, Bode magnitude and Bode phase. The highest specific capacitance ($C_{sp}$) was obtained as $C_{sp} = 286.35\ F \times g^{-1}$ at the scan rate of $20\ mV \times s^{-1}$ for PANI/CuO amongst the PEDOT/CuO ($C_{sp} = 198.89\ F \times g^{-1}$ at $5\ mV \times s^{-1}$) and PPy/CuO ($C_{sp} = 20.78\ F \times g^{-1}$ at $5\ mV \times s^{-1}$) by CV method. Long-term stability of the capacitor has also been tested by CV method, and the results indicated that, after 500 cycles, the specific capacitance of PANI/CuO nanocomposite film is 81.82 % of the initial capacitance. An equivalent circuit model of $R_s(C_{dl}(R_1(Q(R_2W))))$ has been used to fit the experimental and theoretical data.

**Keywords** Electro-synthesis · Pseudocapacitance · CuO nanoparticles · Supercapacitor · Specific capacitance

✉ Murat Ates
mates@nku.edu.tr;
http://mates-en.nku.edu.tr; http://www.atespolymer.org

[1] Department of Chemistry, Faculty of Arts and Sciences, Namik Kemal University, Degirmenalti Campus, 59030 Tekirdag, Turkey

[2] Department of Chemistry and Biochemistry, University of California Los Angeles, Los Angeles, CA 90095, USA

[3] Department of Bioengineering, University of California Los Angeles, Los Angeles, CA 90095, USA

## Introduction

Conducting polymers (CPs) and their nanocomposites are promising candidates for a variety of applications including organic photovoltaics [1], light-emitting diodes [2], field effect transistors [3], gas sensors [4], corrosions [5], memory devices [6], supercapacitors [7, 8], and stretchable electrodes [9–12]. The redox process is used in conducting polymers to store and release charge. This process offers the opportunity of achieving high levels of specific capacitance [13–15]. Faradaic reactions generate a charge transfer pseudocapacitance at the electrode surface. CPs have many advantages, such as compatibility in both aqueous and organic electrolytes and ability to work in wide potential ranges [16, 17].

A wide variety of CPs, such as polyaniline (PANI), poly(3,4-ethylenedioxythiophene) (PEDOT), polypyrrole (PPy) and its nanocomposites, have been investigated as electrode materials in supercapacitors and batteries [18–20]. Polyaniline (PANI) is one of the most widely studied conducting polymers due to its facile synthesis, excellent chemical and environmental stability and good electrical conductivity [21, 22].

Having high capacitance values as a result of their high specific power levels, metal oxides have been extensively used in commercial devices. This also enables them as a material of choice for supercapacitor applications [23, 24]. Conducting polymers and metal oxides are extensively used in pseudocapacitors as electroactive materials [25]. Although high specific capacitance offers long cycle life, it has a limited usage in commercial applications because of its high cost. Materials such as Ir, Co, Mo, Ti, V, Sn, Fe, Cu and metal oxides can be used as electrode materials for supercapacitors [26]. Metal oxides are preferred materials due to their high surface areas, good electrical conductivities, long charge–discharge cycles, high capacitance values and good mechanical properties [27]. Among the metal oxide family, copper oxide (CuO), having a low bandgap (1.2 eV) displays p-type semiconductor behavior and it is one of the most suitable candidates for supercapacitor electrode materials due to its environmental friendly nature and low material costs along with its good pseudocapacitive properties.

Electrochemical impedance spectroscopy (EIS) is one the most efficient and reliable methods for electrochemical characterization of a system which includes double layer capacitance, diffusion impedance, charge transfer and solution resistance measurements [28]. EIS uses two theoretical models, namely, homogeneous [29] and porous [30], to explain the behavior of an electrode which is coated with a polymer layer.

Polymer composites were synthesized using aniline, EDOT, and pyrrole monomers and CuO nanoparticles and were characterized by FTIR and ATR, cyclic voltammetry (CV), SEM and EIS. Cyclic voltammetry and EIS were used to measure the specific capacitance in the aqueous sulfuric acid solution. Stability tests against charge–discharge were also performed using CV for this solution. EIS measurements of equivalent circuit model of $R_s(C_{dl}(R_1(Q(R_2W))))$ are discussed to fit the theoretical and experimental data.

## Experimental

### Materials

Aniline (ANI, 99.5 %), 3,4-ethylenedioxythiophene (EDOT, 97 %), pyrrole (Py, 97 %), sodium dodecylsulfate (SDS), and hexadecyl-3-methylammonium bromide were purchased from Sigma-Aldrich (http://www.sigma-aldrich.com, Steinheim, Germany). Butanol (>98), sulfuric acid ($H_2SO_4$, 96 %), and acetone (ACS, ISO) were purchased from Merck (http://www.merck.de, Darmstadt, Germany). All chemicals were high-grade reagents and were used as received.

### Instrumentation

An Iviumstat Model Potentiostat/Galvanostat (software, iviumsoft and Faraday cage, BASI Cell Stand $C_3$) was used for electrochemical studies which was equipped with a three-electrode electrochemical cell, employing glassy carbon electrode (GCE) as a working electrode (0.07 $cm^2$), platinum disk as a counter electrode (geometric area 0.020 $cm^2$) and a saturated calomel electrode (SCE) as a reference electrode. All potentials are presented on the SCE scale.

Digital microscope (TENSION), ultrasonic bath (Elma, E3OH, Elmasonic), deionized water equipment (purelab Option-Q, ELGA, DV25), accurate balance (OHAUS Pioneer), incubator (DRY-Line, VWR) were used in various experimental steps. The modified electrodes were characterized by scanning electron microscopy (SEM) using a Carl Zeiss Leo 1430 VP and Fourier-transform infrared spectroscopy-attenuated total reflectance (FTIR-ATR) spectrum (Perkin Elmer Spectrum One B) analyses.

### Preparation of carbon fiber microelectrodes (CFME)

A single filament of the CFME was used as a working electrode. All the electrodes were prepared using a 3 cm length of the CFME (diameter $\sim$7 μm) attached to a copper wire with Teflon tape. Only 1.0 cm of the carbon fiber was dipped into the solution to keep the electrode area constant ($\sim$0.002 $cm^2$). The rest of the fiber was covered with the Teflon tape.

### EIS and modeling

The electrochemical impedance spectroscopy (EIS) measurements were recorded at room temperature (25 °C ± 1) using a conventional three electrode cell configuration. EIS measurements were conducted in monomer-free electrolyte solutions with a perturbation amplitude 10 mV over a frequency range of 10 mHz to 100 kHz on Iviumstat Model Potentiostat/Galvanostat (software; iviumsoft). The circuit model parameters were obtained by ZSimpWin 3.22 programme.

### The calculation of specific capacitance with cyclic voltammetry

Cyclic voltammograms and electrochemical impedance spectroscopy data for monomer concentrations of $[ANI]_0 = 0.1$ M, $[EDOT]_0 = 0.1$ M, and $[Py]_0 = 0.1$ M in total solution of 5 mL with 0.2 M $H_2SO_4$ solution were measured and specific capacitances calculated by the following formula, which is given below,

$$\text{Specific capacitance (Sc)} = \Delta Q / M \times \Delta V.$$

In this formula; $\Delta Q$ is the voltammetric charge which integrated from cyclic voltammogram (C), $\Delta V$ is the potential range (V) [31], $M$ is the mass of electrode material on the electrode surface (g) which is calculated from the following formula;

$$M = \left(Q_{\text{deposition}} \times \text{MA}_{\text{monomer}}\right)/Z \times F \quad (1)$$

In this formula; $Q_{\text{deposition}}$ (deposition charge obtained from synthesized by chronoamperometric method, $\text{MA}_{\text{monomer}}$ (g/mol), $Z = 2$ [32], $F = 96{,}485$ C/mol.

Electrochemical impedance spectroscopy was measured in 0.2 M $H_2SO_4$ in monomer-free solution at different scan rates of 5, 10, 20, 30, 40, 50, 60, 70, 80, 90, 100 mV $\times$ $s^{-1}$ for PANI, PEDOT and PPy which were coated with 1 % CuO nanomaterials for 600, 600, and 400 s, respectively.

## Results and discussion

### Electro-synthesis of PANI/CuO, PEDOT/CuO and PPy/CuO nanocomposites

0.15 M SDS was added to 0.20 M $H_2SO_4$ solution. CuO nanomaterials (0.9 mg) were added to the solution until CuO/monomer percent ratio reached 1 %. Ultrasonication was used to enhance the mixing for 45 min. 5 ml of the prepared solution was taken into a separate beaker and aniline monomers were added to this solution until the concentration reached 0.1 M during continuous ultrasonication for 30 min (Fig. 1a).

Before the polymer was formed, the optimal doping conditions for EDOT monomers were studied. A solution of 0.01 M hexadecyltrimethylammonium bromide in 100 ml of butanol supplied the best conditions. CuO nanomaterials (1.4 mg) were added to the solution until CuO/monomer percent ratio reached 1 %. Ultrasonication was used to enhance the mixing for 45 min. 5 ml of the prepared solution was taken into a separate beaker and EDOT monomers were added to this solution until the concentration reached 100 mM during continuous ultrasonication for 30 min (Fig. 1b).

1.2 mg of CuO nanomaterials was added to 0.15 M SDS solution until CuO/pyrrole percent ratio reached 1 %. Ultrasonication was used to enhance the mixing for 45 min. 5 ml of the prepared solution was taken in a polymerization cell and 70 µl of (0.1 M) pyrrole monomers was added to this solution and continuous

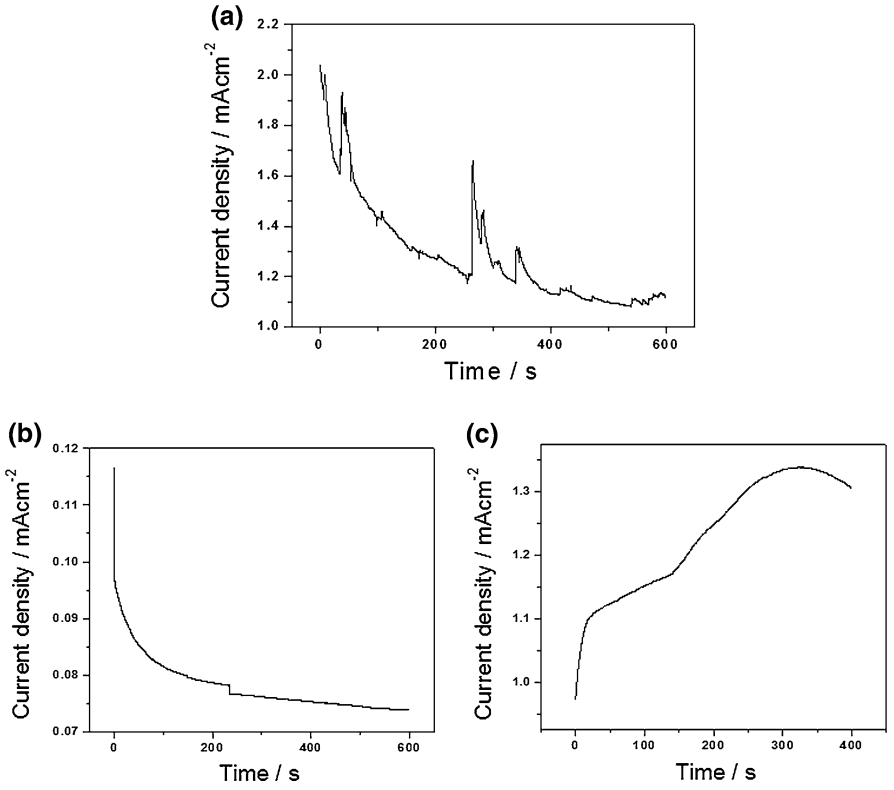


**Fig. 1** Electro-synthesis of **a** ANI/GCE in 0.20 M $H_2SO_4$/0.15 M SDS/1 % CuO solution. $[ANI]_0 = 0.1$ M, at a constant potential of 0.8 V in 600 s, $Q$: $7.719 \times 10^{-1}$ C, **b** EDOT/GCE in 0.01 M hexadecyl 3-methyl ammonium bromide/1 % CuO/butanol solution. $[EDOT]_0 = 100$ mM, at a constant potential 1.2 V in 600 s. $Q$: $3.279 \times 10^{-3}$ C, **c** Py/GCE in 0.1 M SDS/1 % CuO solution. $[Py]_0 = 0.1$ M, at a constant potential of 0.9 V in 400 s. $Q$: $1.019 \times 10^{-1}$ C

ultrasonication was applied for 30 min (Fig. 1c). All PANI/CuO, PEDOT/CuO and PPy/CuO nanocomposite synthesized were electrocoated onto glassy carbon electrode (GCE) using chronoamperometry with a three-electrode setup. Pt was auxiliary electrode whereas Ag/AgCl was used as reference electrode. Polymerization time was performed in 600, 600 and 400 s at constant potentials of 0.8, 1.2 and 0.9 V for PANI/CuO, PEDOT/CuO and PPy/CuO nanocomposites, respectively.

## FTIR-ATR analysis of PANI/CuO, PEDOT/CuO and PPy/CuO nanocomposites

FTIR-ATR analysis for PANI is given in Fig. 2a where the peak at 3216 $cm^{-1}$ refers to N–H stretching, the peaks at 2915 $cm^{-1}$ and 2848 $cm^{-1}$ refer to C–H stretching of the ring structure whereas the one at 1533 $cm^{-1}$ originates from in-ring C=C stretching. The peak at 1204 $cm^{-1}$ is bifurcated, showing the secondary amine

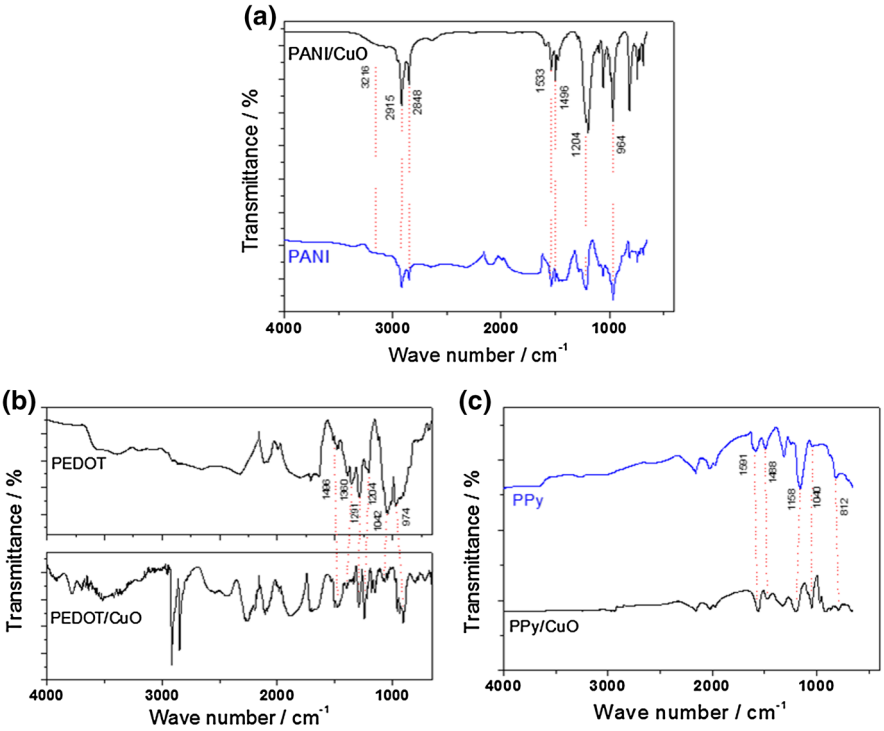


**Fig. 2** FTIR-ATR spectra for **a** PANI and PANI/CuO, **b** PEDOT and PEDOT/CuO, **c** PPy and PPy/CuO

stretching of C–N. The peak at 964 $cm^{-1}$ refers to C=H alkene peaks. The spectrum for PANI/CuO was found to be similar to that of PANI.

The FTIR-ATR spectrum for PEDOT (Fig. 2b) shows two striking peaks at 1496 $cm^{-1}$ and 1360 $cm^{-1}$ corresponding to non-symmetrical in-ring stretching of C=C and C–C. The peaks at 1291, 1204 and 1042 $cm^{-1}$ refer to C–O–C bond stretching in ethylene dioxide ring. The peak at 944 $cm^{-1}$ corresponds to the C–S–C stretching in thiophene ring. In the literature, the absorptions at 513.3 and 592.7 $cm^{-1}$ are the characteristic stretching vibrations of Cu–O bond in monoclinic CuO [33, 34]. This change is due to loss in conjugation and molecular order after modification of PEDOT with CuO [35]. Such kind of new peak formations and shifting of the peaks could be due to the fact that some of the inorganic CuO was incorporated in the polymer matrix.

The FTIR-ATR spectrum for PPy (Fig. 2c) shows peaks at 1591 $cm^{-1}$ and 1488 $cm^{-1}$ which refer to non-symmetrical in-ring stretching of C=C bond. The peaks at 1158 $cm^{-1}$ and 1040 $cm^{-1}$ represent the C–N stretching arising from the polypyrrole skeleton. The peak at 812 $cm^{-1}$ refers to the characteristic C–H bond stretching of the polypyrrole. The spectrum for PPy/CuO was found to be similar to that of PPy.

## SEM–EDX analysis

Scanning electron microscopy images of homopolymers of PANI, PEDOT and PPy and their nanocomposites of PANI/CuO, PEDOT/CuO and PPy/CuO were performed on CFMEs as shown in Fig. 3a–f. We obtained the homogeneous films for homopolymers. By addition of CuO nanomaterials, film surface has also homogeneous surface morphology. The coatings with micro-spherical morphology were formed using the solution of 0.2 M $H_2SO_4$ solution. Many process parameters, such as the applied voltage, initial monomer concentration, electrolyte type and concentration, and the polymerization time affect the surface energy of the electro-coated fiber.

## Supercapacitor behaviors of PANI/CuO, PEDOT/CuO and PPy/CuO nanocomposites

The redox behavior of polymer/CuO composite electrodes was investigated in 0.5 M $H_2SO_4$ in the potential window of 0–0.8 V (Fig. 4).

As the scan rate decreases from 100 to 5 mV $\times$ $s^{-1}$, the graph for CV measurement approaches to a rectangular shape and the specific capacitance values increase. The highest specific capacitance for PANI/CuO nanocomposite was found to be $C_{sp} = 286.35$ F $\times$ $g^{-1}$ at a scan rate of 20 mV $\times$ $s^{-1}$.

The charge storage in CuO was mainly based on the Faradaic reaction of copper oxide according to a pseudocapacitive mechanism [36]. The main pseudocapacitance behavior of the sample can be attributed to the following quasi-reversible redox transition of $Cu^{+2}$–$Cu^{+1}$ (0.46 V) and vice versa (0.52 V), in agreement with the literature [37]

$$2CuO + 2H^+ + 2e^- \leftrightarrow Cu_2O + H_2O. \quad (2)$$

The redox behavior of PANI/CuO nanocomposite film was investigated in monomer-free solution and it was found to display diffusion-controlled behavior according to Randles–Sevcik equation

$$I_p = \left(2.69 \times 10^5\right) \times A \times D^{1/2} \times C_0 \times v^{1/2}. \quad (3)$$

In this formula; $v$ is the scan rate, $A$ is the electrode area, $D$ is the diffusion coefficient of electroactive species, $C_0$ is the concentration. Peak current ($I_p$) is directly proportional with square root of scan rate ($v^{1/2}$), which shows diffusion-controlled redox behavior. If the $I_p$ is directly proportional to scan rate ($v$), it shows thin layer behavior (Table 1).

The redox behavior of PANI/CuO, PEDOT/CuO and PPy/CuO nanocomposite films was investigated in monomer-free solution using CV measurements with respect to different scan rates and they were found to display a diffusion-controlled behavior (Table 2). We compared the specific capacitance values at different scan rates and observed that the highest capacitance value of $C_{sp} = 198.89$ F $\times$ $g^{-1}$ was reached the slowest scan rate. The decrease in capacitance for PEDOT/CuO

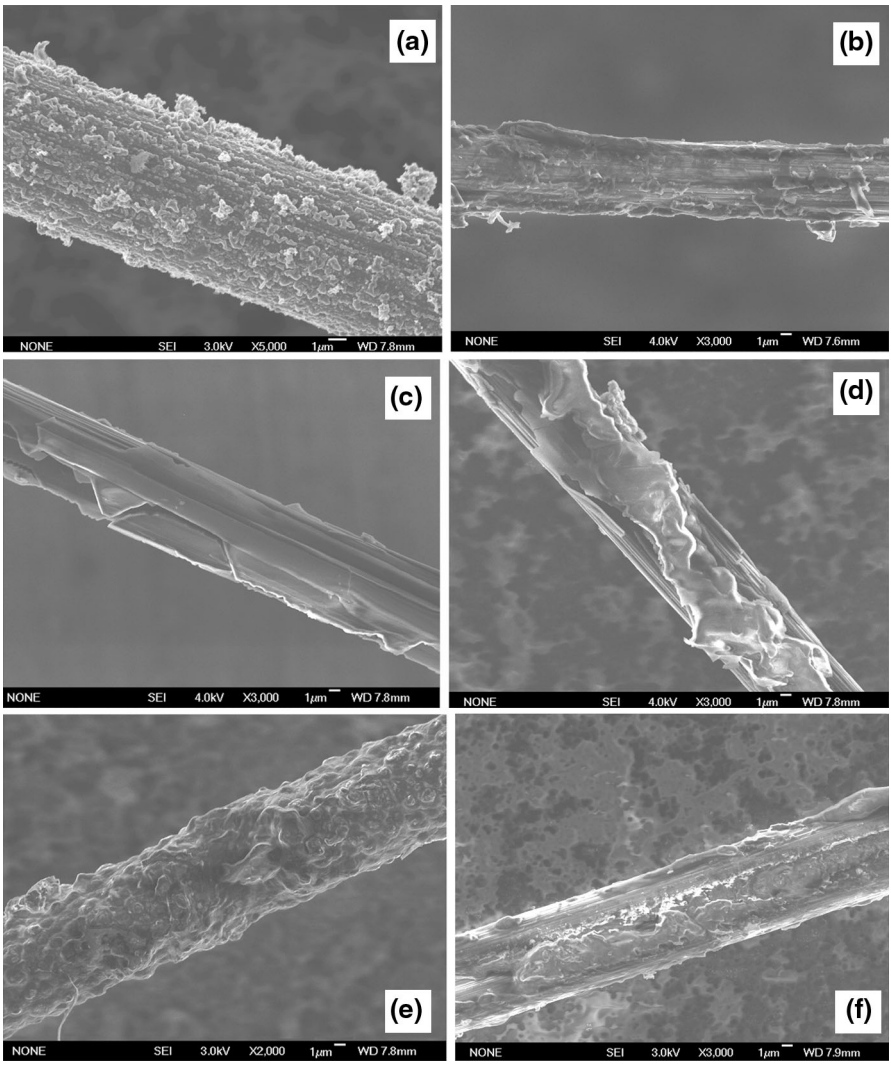


**Fig. 3** SEM images for **a** PANI, **b** PANI/CuO, **c** PEDOT, **d** PEDOT/CuO, **e** PPy, **f** PPy/CuO

compared to PANI/CuO nanocomposite films could be attributed to the decrease in surface area due to the growth of polymer film on the substrate or the change in the potential window.

The highest specific capacitance ($C_{sp}$) of PANI/CuO nanocomposite films was obtained as 286.35 F $\times$ $g^{-1}$ at 20 mV $\times$ $s^{-1}$. The highest $C_{sp}$ was obtained as $C_{sp}$ = 198.89 F $\times$ $g^{-1}$ for PEDOT/CuO at 5 mV $\times$ $s^{-1}$ and $C_{sp}$ = 20.78 F $\times$ $g^{-1}$ for PPy/CuO nanocomposite films at 5 mV $\times$ $s^{-1}$ (Table 2).

In the literature, graphene oxide (GO)/CuO nanocomposites have the specific capacitance of $C_{sp}$ = 245 F $\times$ $g^{-1}$ at current density of 0.1 A $\times$ $g^{-1}$ compared to

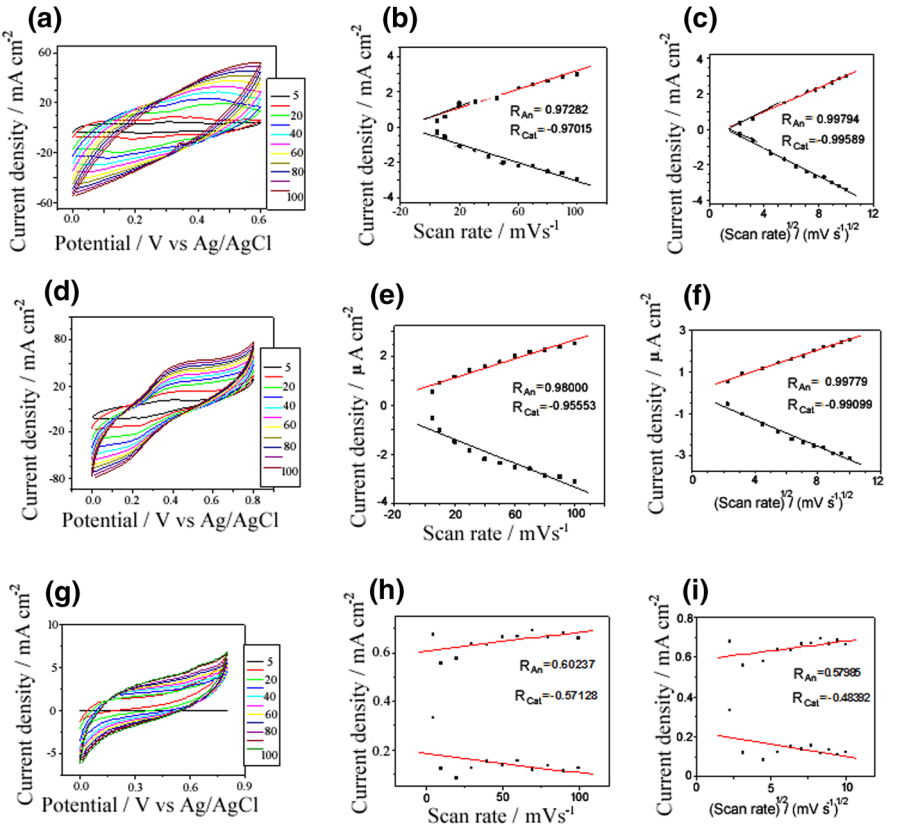


**Fig. 4** **a** PANI/CuO/GCE, **b** scan rate vs current density of PANI/CuO, **c** $(\text{scan rate})^{1/2}$ vs current density of PANI/CuO, **d** PEDOT/CuO/GCE, **e** scan rate vs current density of PEDOT/CuO, **f** $(\text{scan rate})^{1/2}$ vs current density of PEDOT/CuO, **g** PPy/CuO/GCE, **h** scan rate vs current density of PPy/CuO, **i** $(\text{scan rate})^{1/2}$ vs current density of PPy/CuO, in 0.5 M $H_2SO_4$ monomer-free solution at a scan rate of 5, 10, 20, 30, 40, 50, 60, 70, 80, 90, 100 mV × $s^{-1}$, potential window between 0–0.6 V and 0–0.8 V

**Table 1** Redox behaviors of scan rate vs current density and square root of scan rate vs current density values for PANI/CuO, PEDOT/CuO, and PPy/CuO nanocomposites

| Nanocomposites | Scan rate/current density | | $(\text{Scan rate})^{1/2}$/current density | | Redox behavior |
|---|---|---|---|---|---|
| | $R_{An}$ | $R_{Cat}$ | $R_{An}$ | $R_{Cat}$ | |
| PANI/CuO | 0.97282 | −0.97015 | 0.99794 | −0.99589 | Diffusion cont. |
| PANI/CuO | 0.98000 | −0.95553 | 0.99779 | −0.99099 | Diffusion cont. |
| PANI/CuO | 0.60237 | −0.57128 | 0.57985 | 0.48392 | Thin film |

the pure components (125 F × $g^{-1}$ for CuO and 120 F × $g^{-1}$ for GO) and the layer by layer coated electrodes (155 F × $g^{-1}$) [38]. Our $C_{sp}$ values for PANI/CuO nanocomposite films obtained from CV ($C_{sp}$ = 286.35 F × $g^{-1}$ at 20 mV × $s^{-1}$) and EIS ($C_{sp}$ = 286.317 F × $g^{-1}$) measurements are higher than the GO/CuO nanocomposite films.

**Table 2** Capacitance values at different scan rates for PANI/CuO, PEDOT/CuO and PPy/CuO nanocomposites

| PANI/CuO | | PEDOT/CuO | PPy/CuO |
|---|---|---|---|
| Scan rate ($mVs^{-1}$) | $C_{sp}$ ($F \times g^{-1}$) | $C_{sp}$ ($F \times g^{-1}$) | $C_{sp}$ ($F \times g^{-1}$) |
| 5 | 276.56 | 198.89 | 20.78 |
| 10 | 261.72 | 134.85 | 6.52 |
| 20 | 286.35 | 87.23 | 2.57 |
| 30 | 247.34 | 69.41 | 1.51 |
| 40 | 243.46 | 59.46 | 1.16 |
| 50 | 238.93 | 52.28 | 0.99 |
| 60 | 235.09 | 46.96 | 1.05 |
| 70 | 227.82 | 42.56 | 0.80 |
| 80 | 219.32 | 39.19 | 0.74 |
| 90 | 209.93 | 36.61 | 0.73 |
| 100 | 200.023 | 34.44 | 0.68 |

## Electrochemical impedance spectroscopy of PANI/CuO, PEDOT/CuO and PPy/CuO nanocomposite films

The electrical properties of a supercapacitor are determined by the selection of electrode material [39]. In this study, electric double layer capacitance (EDLC) materials and processes for cell were constructed with polymer and metal oxides of CuO. The choice of electrolyte in an EDLC device is very important for the electrode material that we used the 0.5 M $H_2SO_4$ solution. In all EIS studies, Nyquist plot revealed a depressed small semicircle at high-frequency region, which is caused by the parallel combination of resistive and capacitive components of the electrode material, and a low-frequency spike which shows an inclination [40]. The low-frequency capacitance ($C_{sp}$) values of polymer and polymer/CuO nanocomposite films (at 0.01 Hz) were calculated by the equation of

$$C_{sp} = (2 \times \pi \times f \times Z_{im})^{-1} \quad (4)$$

where $C_{sp}$ is the specific capacitance, ($Z_{im}$) is the slope of a plot of the imaginary component of impedance versus the inverse of the frequency ($f$) [41, 42]. A low frequency, the imaginary part of the impedance sharply increases (as a vertical line) giving the characteristic of capacitive behavior [43]. The highest specific capacitance value was obtained as $C_{sp} = 286.317\ F \times g^{-1}$ for PANI/CuO films (Fig. 5a, b). This value is also very close value obtained from CV capacitance calculations ($C_{sp} = 286.35\ F \times g^{-1}$) as shown in Table 2. These results may be attributed to that all of the other samples have high charge density at the electrolyte solution which results in high resistance of ion transfer and, therefore, low capacitances for PEDOT/CuO ($C_{sp} = 198.86\ F \times g^{-1}$) and PPy/CuO ($C_{sp} = 0.490\ F \times g^{-1}$).

The composite preparation from PANI/CuO nanocomposite produces a hybrid material having great mechanical strength, high capacitance properties, electrical

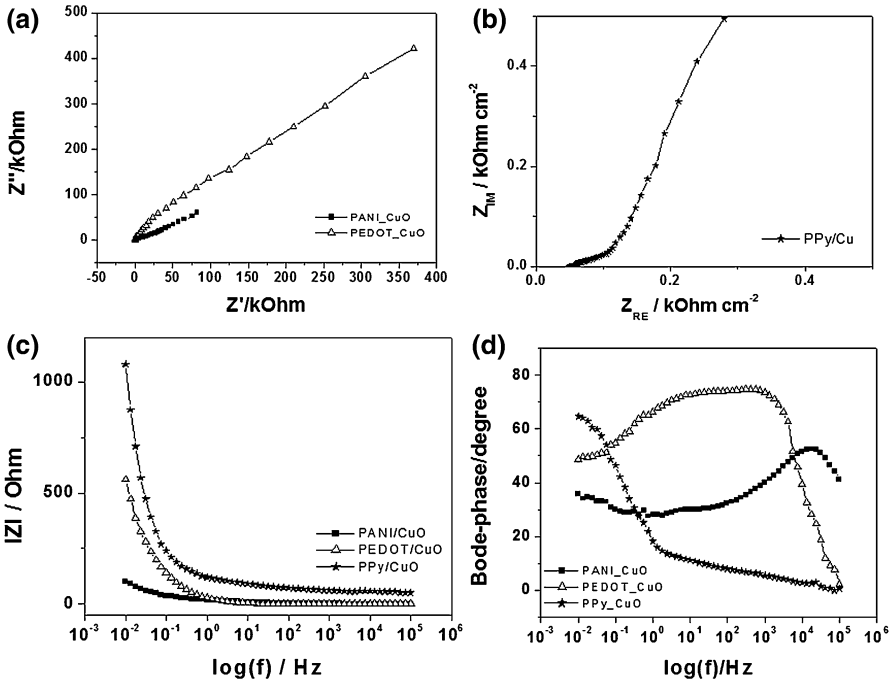


**Fig. 5** **a** Nyquist plot for PANI/CuO and PEDOT/CuO, **b** Nyquist plot for PPy/CuO, **c** Bode-magnitude, **d** Bode-phase plots. All measurements were taken in 0.5 M $H_2SO_4$ solution, 10 mV amplitude, the frequency range between 10 mHz to 100 kHz

properties and good processability [44, 45]. A value of double layer capacitance ($C_{dl}$) was calculated from a Bode-magnitude plot by extrapolating the linear section to a value of $\omega = 1$ ($\log\omega = 0$) and employing the relationship

$$\mathrm{IZI} = 1/C_{dl} \tag{5}$$

as given in Fig. 5c. The $C_{dl}$ value was obtained as $C_{dl} = 0.150\ \mathrm{F} \times \mathrm{g}^{-1}$ for PANI/CuO, PEDOT/CuO and PPy/CuO nanocomposite films. $C_{dl}$ changes with electrolyte type and diffusion rate.

The Bode-phase plot was taken by changing the frequency range from 10 mHz to 100 kHz for PANI/CuO, PEDOT/CuO and PPy/CuO nanocomposite films as shown in Fig. 5d. The phase angle was obtained as $\theta = 52.43^{\circ}$ at frequency of $f = 17{,}367.12$ Hz.

The specific capacitance ($C_{sp}$), double layer capacitance ($C_{dl}$) and phase angle ($\theta$) values of PANI/CuO, PEDOT/CuO and PPy/CuO nanocomposites are given in Table 3. The highest $C_{sp}$ was obtained as $C_{sp} = 286.17\ \mathrm{F} \times \mathrm{g}^{-1}$ for PANI/CuO nanocomposite films. However, the highest double layer capacitance ($C_{dl}$) and phase angle ($\theta$) were obtained as $C_{dl} = 11.55\ \mathrm{F} \times \mathrm{g}^{-1}$ and $\theta = 74.61^{\circ}$ at 600.39 Hz for PEDOT/CuO nanocomposite films. We conclude that PPy/CuO nanocomposite

**Table 3** Specific capacitance, double layer capacitance and phase angle values of PANI/CuO, PEDOT/CuO and PPy/CuO nanocomposites

| Nanocomposites | $C_{sp}$ (F × g$^{-1}$) | $C_{dl}$ (F × g$^{-1}$) | $\theta$ (Phase angle) |
|---|---|---|---|
| PANI/CuO | 286.17 | 0.15 | 52.43° (17,367.12 Hz) |
| PEDOT/CuO | 198.86 | 11.55 | 74.61° (600.39 Hz) |
| PPy/CuO | 0.490 | 0.0008 | 64.42° (0.0103 Hz) |

films have the lowest $C_{sp}$, and $C_{dl}$ values amongst the PANI/CuO and PEDOT/CuO nanocomposite films.

## Stability tests of PANI/CuO, PEDOT/CuO and PPy/CuO nanocomposites

The specific capacitance of PANI/CuO film was measured in 0.5 M $H_2SO_4$ solution at 500 cycles from CV measurements. The $C_{sp}$ value was decreased from $C_{sp} = 200.58$ F × g$^{-1}$ to 164.12 F × g$^{-1}$ as shown in Fig. 6a. Long-term stability of the capacitor has also been tested by CV method, and the results indicated that, after 500 cycles, the $C_{sp}$ of PANI/CuO nanocomposite film is 81.82 % of the initial capacitance. There is a big decrease in the $C_{sp}$ value up to 100 cycle, after that cycle, The $C_{sp}$ value slowly decreases for PEDOT/CuO nanocomposite films as shown in Fig. 6b. $C_{sp}$ of PEDOT/CuO nanocomposite film is 68.55 % of the initial

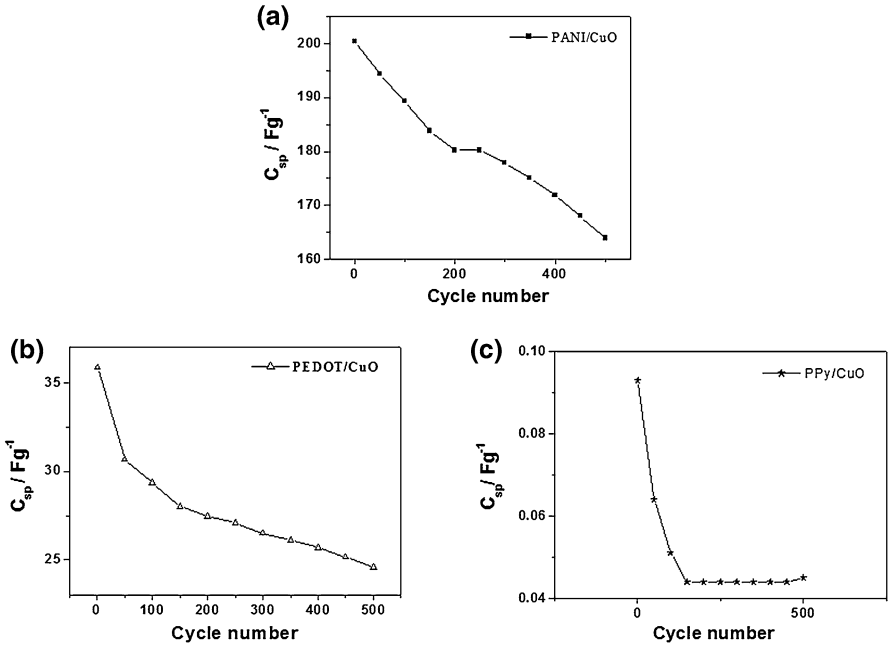


**Fig. 6** Stability tests of **a** PANI/CuO, **b** PEDOT/CuO and **c** PPy/CuO. All measurements were taken in 0.5 M $H_2SO_4$ solution, 500 cycle and scan rate of 100 mVs$^{-1}$

capacitance. There is a sharp decrease for PPy/CuO nanocomposite film up to 150 cycles. After that cycle, $C_{sp}$ value is stable up to 500 cycles as shown in Fig. 6c. $C_{sp}$ of PPy/CuO nanocomposite film is 48.39 % of the initial capacitance.

## Equivalent circuit model evaluation of PANI/CuO, PEDOT/CuO and PPy/CuO nanocomposites

The equivalent electrical circuit model of $R_s(C_{dl}(R_1(Q(R_2W))))$ was given for the electrolyte/PANI or PEDOT or PPy/CuO/GCE system to a frequency of 0.01 Hz to 100 kHz as shown in Fig. 7. The ZSimpWin 3.22 circuit model program from Princeton Applied Research was evaluated to fit the theoretical and experimental circuits. Kramers–Kronig (K–K) transforms were performed in the analysis of impedance data with reference to the conditions of stability and linearity [46].

The electrochemical parameters obtained from fitting the impedance data to the $R_s(C_{dl}(R_1(Q(R_2W))))$ circuit are shown in Fig. 8.

In the circuit, $R_s$ represents the solution resistance, $C_{dl}$ is the double layer capacitance, $R_1$ is the nanocomposite film resistance, $R_2$ is the charge transfer resistance, $W$ is

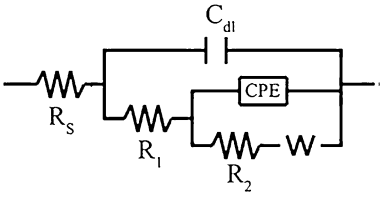


**Fig. 7** Equivalent circuit model of $R_s(C_{dl}(R_1(Q(R_2W))))$ for PANI/CuO, PEDOT/CuO and PPy/CuO nanocomposites

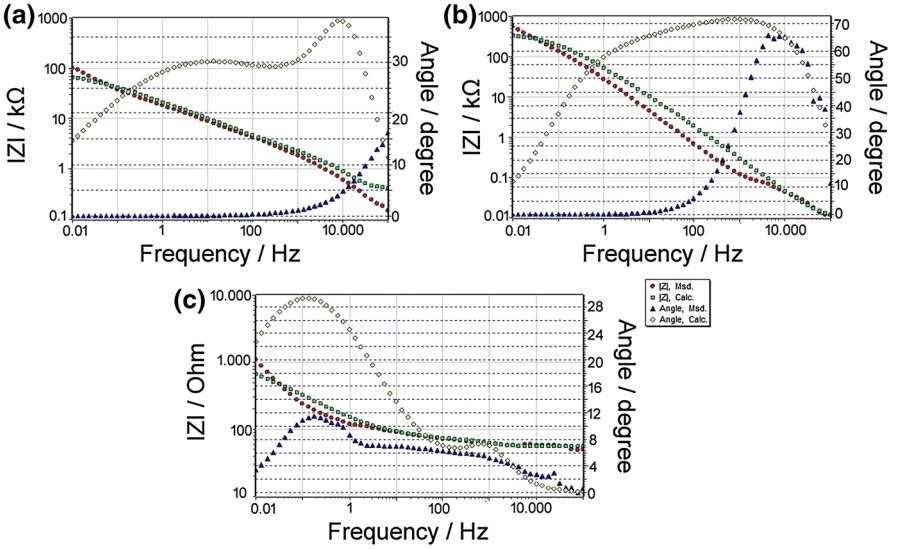


**Fig. 8** Theoretical and experimental data obtained from equivalent circuit model of $R_s(C_{dl}(R_1(Q(R_2W))))$ for Bode-magnitude plots **a** PANI/CuO, **b** PEDOT/CuO, **c** PPy/CuO nanocomposites

**Table 4** $R_s(C_{dl}(R_1(Q(R_2W))))$ equivalent circuit model parameter values for PANI/CuO, PEDOT/CuO and PPy/CuO nanocomposites

| Circuit parameters | PANI/CuO | PEDOT/CuO | PPy/CuO |
|---|---|---|---|
| $R_S$ ($\Omega \times cm^2$) | 89.84 | 11.28 | 58.75 |
| $C_{dl}$ ($\mu F \times cm^{-2}$) | $1.407 \times 10^{-2}$ | $9.767 \times 10^{-1}$ | 70.68 |
| $R_1$ ($\Omega \times cm^2$) | $4.68 \times 10^{-4}$ | 7.86 | 33.4 |
| CPE; $Y_o$ ($\mu S\ s^{-n} \times cm^{-2}$) | $1.90 \times 10^4$ | $7.16 \times 10^{-2}$ | 70.1 |
| $n$ | 0.67 | 0.75 | 0.71 |
| $R_2$ ($k\Omega \times cm^2$) | 3685 | 310.7 | 1447 |
| $W$; $Y_o$ ($\mu S\ s^{-0.5} \times cm^{-2}$) | $1.637 \times 10^4$ | 5.73 | $2.09 \times 10^{-3}$ |
| $\chi^2$ | $1.59 \times 10^{-3}$ | $3.15 \times 10^{-3}$ | $7.10 \times 10^{-3}$ |

Warburg impedance, which shows the ion diffusion and CPE is the constant phase element ($Q$). The CPE as a distributed circuit element was obtained from equation:

$$Z_{CPE} = T^{-1}(j\omega)^{-n} \quad (6)$$

where $T$, $\omega$ and $n$ are the CPE coefficient, the angular frequency and the exponent, respectively. The $n$ value is 0 and 1. In the case of $n = 0$, the CPE shows an ideal resistance, when $n = 0.5$, it denotes diffusion behavior; and at $n = 1$, the CPE is equivalent to pure capacitance (Table 4). The values obtained for n after each modification step are close to 1, indicating that the CPE exhibited capacitance behavior that is characteristic of PANI/CuO, PEDOT/CuO and PPy/CuO nanocomposite electrodes. The highest solution resistance ($R_s$) was obtained as $R_s = 89.84\ \Omega \times cm^2$ for PANI/CuO nanocomposite films compared to $R_s = 11.28\ \Omega \times cm^2$ for PEDOT/CuO film and $R_s = 58.75\ \Omega \times cm^2$ for PPy/CuO nanocomposite films. The highest double layer capacitance ($C_{dl}$) was obtained as $C_{dl} = 70.68\ \mu F \times cm^{-2}$ for PPy/CuO nanocomposite films. In addition, the highest charge transfer resistance ($R_2$) was obtained as $R_2 = 3685\ k\Omega \times cm^2$ for PANI/CuO nanocomposite films. The results were also supported by the specific capacitances ($C_{sp} = 286.35\ F \times g^{-1}$) at $20\ mV \times s^{-1}$ obtained from CV measurements and $C_{sp} = 286.317\ F \times g^{-1}$ obtained from EIS measurements. $C_{sp}$ values are the highest amongst the PEDOT/CuO and PPy/CuO nanocomposite films.

## Conclusions

Nowadays, the demand on supercapacitors has increased due to energy storage devices compared to lithium ion batteries. Pseudocapacitors were obtained as nanocomposites together with metal oxides and conducting polymers. In this study, we have studied supercapacitor behavior of a novel nanocomposite of PANI/CuO, PEDOT/CuO and PPy/CuO films. The specific capacitances were comparatively studied in 0.2 M $H_2SO_4$ solution at different scan rates (5, 10, 20, 30, 40, 50, 60, 70, 80. 90 and 100 $mV \times s^{-1}$) by CV method. The highest $C_{sp}$ was obtained as $C_{sp} = 286.35\ F \times g^{-1}$ for PANI/CuO at $20\ mV \times s^{-1}$ amongst the

$C_{sp} = 198.89\ F \times g^{-1}$ for PEDOT/CuO at $5\ mV \times s^{-1}$ and $C_{sp} = 20.78\ F \times g^{-1}$ for PPy/CuO at $5\ mV \times s^{-1}$. The EIS results also support the $C_{sp}$ values obtained from CV method. The highest $C_{sp}$ was obtained from Nyquist plot as $C_{sp} = 286.317\ F \times g^{-1}$ for PANI/CuO films. The long-term stability tests (500 cycles) were successfully performed by CV method measurements for PANI/CuO, PEDOT/CuO and PPy/CuO nanocomposite films. The equivalent circuit model of $R_s(C_{dl}(R_1(Q(R_2W)))$ was used to fit the theoretical and experimental data. The PANI/CuO nanocomposites are, therefore, ideal candidates for electrode materials compared to PEDOT/CuO and PPy/CuO nanocomposites for the development of high-performance, high-power and supercapacitor devices. In future, PANI/CuO, PEDOT/CuO and PPy/CuO will be synthesized for copolymer formations and their supercapacitor behaviors will be studied.

**Acknowledgments** The financial support from Namik Kemal University, Tekirdag, Turkey, project number: NKUBAP.00.10.AR.14.11 is gratefully acknowledged. Authors thank Serhat Tıkız (Afyon Kocatepe Uni., TUAM, Afyon, Turkey) for recording SEM measurements. Authors also thank Dr. Argun Gokceoren (ITU, Istanbul, Turkey) for FTIR-ATR measurements.

**Conflict of interest** Authors must disclose all relationships or interests that could have direct or potential influence or impart bias on the work. Although an author may not feel there is any conflict, disclosure of relationships and interests provides a more complete and transparent process, leading to an accurate and objective assessment of the work. Awareness of a real or perceived conflicts of interest is a perspective to which the readers are entitled. There is not meant to imply that a financial relationship with an organization that sponsored the research or compensation received for consultancy work is appropriate. Examples of potential conflicts of interests that are directly or indirectly related to the research may include but are not limited to the following: research grants from funding agencies (Project Number: NKUBAP.00.10.AR.14.11).

## References

1. Kim SY, Lee KH, Chin BD, Yu JW (2009) Network structure organic photovoltaic devices prepared by electrochemical copolymerization. Sol Energy Mater Sol Cells 93(1):129–135
2. Kasama D, Takata R, Kajii H, Ohmori Y (2009) Optical property of poly(9,9-dioctylfluorene) gel with β phase and application to polymer light emitting diode. Thin Solid Films 518(2):559–562
3. Ciobotaru IC, Matei E, Ciobotaru CC, Polosan S (2014) Embedding of IrQ(ppy)(2) or organometallic compounds in polypyrrole conducting polymer for OLED's applications. Synth Met 198:323–328
4. Inzelt G, Pineri M, Schultze JW, Vorotyntsev MA (2000) Electron and proton conducting polymers: recent developments and prospects. Electrochim Acta 45(15–16):2403–2421
5. Yeh JM, Chen CL, Chen YC, Ma CY, Lee KR, Wei Y, Li S (2002) Enhancement of corrosion protection effect of poly(0-ethoxyaniline) via the formation of poly(*o*-ethoxyaniline)-clay nanocomposite materials. Polymer 43(9):2729–2736
6. He H, Zhu J, Tao NJ, Nagahara LA, Amlani I, Tusi R (2001) A conducting polymer nanojunction switch. J Am Chem Soc 123(31):7730–7731
7. Frackowiak E, Khomenko V, Jurewicz K, Lota K, ḂEguin F (2006) Supercapacitors based on conducting polymers/nanotubes composites. J Power Sources 153(2):413–418
8. Ates M, Uludag N, Karazehir T (2012) Copolymer formation of 9-(2 (benzyloxy) ethyl)-9*H*-carbazole and 1-tosyl-1*H*-pyrrole coated on glassy carbon electrode and electrochemical impedance spectroscopy. J Solid State Electrochem 16(8):2639–2649
9. Chen HY, Hou JH, Zhang SQ, Liang YY, Yang GW, Yang Y, Yu LP, Wu Y, Li G (2009) Polymer solar cells with enhanced open-circuit voltage and efficient. Nat Photonics 3(11):649–653

10. Lipomi DJ, Bao ZA (2011) Stretchable, elastic materials and devices for solar energy conversion. Energy Environ Sci 4(9):3314–3328
11. Sasabe H, Takamatsu J, Motoyama T, Watanabe S, Wagenblast G, Langer N, Molt O, Fuchs E, Lennartz C, Kido J (2010) High-efficiency blue and white organic light-emitting devices incorporating a blue iridium carbene complex. Adv Mater 22(44):5003–5007
12. Kim FS, Ren GQ, Jenekhe SA (2011) One-dimensional nanostructures of pi-conjugated molecular systems: assembly, properties, and applications from photovoltaics, sensors, and nanophotonics to nanoelectronics. Chem Mater 23:682–732
13. Mastragostino M, Arbizzani C, Soavi F (2002) Conducting polymers as electrode materials in supercapacitors. Solid State Ionics 148(3–4):493–498
14. Guimard NK, Gomez N, Schmidt CE (2007) Conducting polymers in biomedical engineering. Prog Polym Sci 32(8–9):876–921
15. Ates M, Uludag N, Karazehir T (2012) Electrolyte effects of poly(3-methylthiohene) via PET/ITO and synthesis of 5-(3,6-di(thiophene-2-yl)-9*H*-carbazole-9-yl) pentanitrile on electrochemical impedance spectroscopy. J Appl Polym Sci 125(4):3302–3312
16. Arbizzani C, Mastragostino M, Meneghello L, Paraventi R (1996) Electronically conducting polymers and activated carbon: electrode materials in supercapacitor technology. Adv Mater 8(4):331–334
17. Mastragostino M, Paraventi R, Zanelli A (2000) Supercapacitors based on composite polymer electrodes. J Electrochem Soc 147(9):3167–3170
18. Snook GA, Kao P, Best AS (2011) Conducting polymer based supercapacitor devices and electrodes. J Power Sources 196(1):1–12
19. Ramya R, Sivasubramanian R, Sangaranarayanan MV (2013) Conducting polymers-based electrochemical supercapacitors-Progress and prospects. Electrochim Acta 101:109–129
20. Pan L, Qiu H, Dou C, Li Y, Pu L, Xu J, Shi Y (2010) Conducting polymer nanostructures: template synthesis and applications in energy storage. Int J Mol Sci 11:2636–2657
21. Li D, Huang JX, Li D, Kaner RB (2009) Polyaniline nanofibers: a unique polymer nanostructure for versatile applications. Acc Chem Res 42(1):135–145
22. Tran HD, Li D, Kaner RB (2009) One-dimensional conducting polymer nanostructures: bulk synthesis and applications. Adv Mater 21(14–15):1487–1499
23. Barsoukov E, Macdonald JR (2005) Impedance spectroscopy: theory, experiment, and applications. In: (ed) Hoboken, Wiley-Interscience, New York, pp 121
24. Lang G, Inzelt G (1999) An advanced model of the impedance of polymer film electrodes. Electrochim Acta 44:2037–2051
25. Ma R, Bando Y, Zhang L, Sasaki T (2004) Layered $MnO_2$ nanobelts: hydrothermal synthesis and electrochemical measurements. Adv Mater 16(11):918–922
26. Bisquert J, Garcia-Belmonte G, Fabregat-Santiago F, Ferriols NS, Bogdanoff P, Pereira EC (2000) Doubling exponent models for the analysis of porous film electrodes by impedance. Relaxation of $TiO_2$ nanoporous in aqueous solution. J Phys Chem B 104(10):2287–2298
27. Wu MS, Huang YA, Yang CH, Jow JJ (2007) Electrodeposition of nanoporous nickel oxide film for electrochemical capacitors. Int J Hydrogen Energy 32(17):4153–4159
28. Wahdame B, Candusso D, Francois X, Harel F, Kauffmann JM, Coquery G (2009) Design of experiment techniques for fuel cell characterization and development. Int J Hydrogen Energy 34(2):967–980
29. Sen P, De A (2010) Electrochemical performances of poly(3,4-ethylenedioxythiophene)-NiFe(2)O(4) nanocomposite as electrode for supercapacitor. Electrochem Acta 55(16):4677–4684
30. Liu C, Ma LP, Cheng HM (2010) Advanced materials for energy storage. Adv Mater 22(8):E28–E62
31. Dhibar S, Sahoo S, Das CK (2013) Fabrication of transition-metal-doped polypyrrole/multiwalled carbon nanotubes nanocomposites for supercapacitor applications. J Appl Polym Sci 130:554–562
32. Aradilla D, Estrany F, Alemán C (2011) Symmetric supercapacitors based on multilayers of conducting polymers. J Phys Chem C 115(16):8430–8438
33. Dubal DP, Dhawale DS, Salunkhe RR, Jamdade VS, Lokhande CD (2005) Fabrication of copper oxide multilayer nanosheets for supercapacitor application. J Alloy Compd 492:26–30
34. Xu YY, Chen DR, Jiao XL (2005) Fabrication of CuO pricky microspheres with tunable size by a simple solution route. J Phys Chem B 109:13561–13566
35. Jundale DM, Navale ST, Khuspe GD, Dalavi DS, Patil PS, Patil VB (2013) Polyaniline–CuO hybrid nanocomposites: synthesis, structural, morphological, optical and electrical transport studies. J Mater Sci Mater Electron 24:3526–3535

36. Dubal VD, Dhawale DS, Salunkhe RR, Jamdade VS, Lokhande CD (2010) Fabrication of copper oxide multilayer nanosheets for supercapacitors application. J Alloys Compd 492:26–30
37. Patake VD, Joshi SS, Lokhande CD, Joo OS (2009) Electrodeposited porous and amorphous copper oxide film for application in supercapacitor. Mater Chem Phys 114:6–9
38. Pendashteh A, Mousavi MF, Rahmanifar MS (2013) Fabrication of anchored copper oxide nanoparticles on graphene oxide nanosheets via an electrostatic coprecipitation and its application as supercapacitor. Electrochim Acta 88:347–357
39. Sharma P, Bhatti TS (2010) A review on electrochemical double-layer capacitors. Energy Convers Manag 51(12):2901–2912
40. Kumar A, Singh RK, Singh HK, Srivastava P, Singh R (2014) Enhanced capacitance and stability of *p*-toluenesulfonate doped polypyrrole/carbon composite for electrode application in electrochemical capacitors. J Power Sources 246:800–807
41. Fiordiponti P, Pistoia G (1989) An impedance study of polyaniline films in aqueous and organic solutions. Electrochim Acta 34(2):215–221
42. Guler FG, Gilsing HD, Schulz B, Sarac AS (2012) Impedance and morphology of hydroxy- and chloro-functionalized poly(3,4-propylenedioxythiophene) nanostructures. J Nanosci Nanotechnol 12(10):7869–7878
43. Sarac AS, Gilsing HD, Gencturk A, Schulz B (2007) Electrochemically polymerized 2,2-dimethyl-3,4-propylenedioxythiohene on carbon fiber for microsupercapacitor. Prog Org Coat 60(4):281–286
44. Qian D, Dickey EC, Andrews R, Rantell T (2000) Load transfer and deformation mechanisms in carbon nanotube-polystyrene composites. Appl Phys Lett 76(20):2868–2870
45. Shi SL, Zhang LZ, Li JS (2009) Electrical and dielectric properties of multiwall carbon nanotube/polyaniline composites. J Polym Res 16(4):395–399
46. Urquidimacdonald M, Real S, Macdonald DD (1990) Applications of Kramers–Kronig transform in the analysis of electrochemical impedance data 3. Stability and linearity. Electrochim Acta 35(10):1559–1566